Postharvest Biology and Technology 188 (2022) 111895

Contents lists available at ScienceDirect

Postharvest Biology and Technology

journal homepage: www.elsevier.com/locate/postharvbio

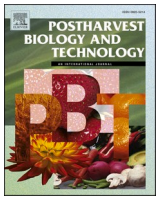

Non-destructive follow-up of 'Jintao' kiwifruit ripening through VIS-NIR spectroscopy – individual vs. average calibration model's predictions

Andreia M. Afonso [a], Maria D. Antunes [b], Sandra Cruz [a], Ana M. Cavaco [a], Rui Guerra [a,c,*]

[a] CEOT, Universidade do Algarve, Campus de Gambelas, 8005-189 Faro, Portugal
[b] MED, Universidade do Algarve, Campus de Gambelas, 8005-189 Faro, Portugal
[c] Departamento de Física, Faculdade de Ciências e Tecnologia, Universidade do Algarve, Campus de Gambelas, 8005-189 Faro, Portugal

ARTICLE INFO

Keywords:
Noninvasive
Internal quality
Optimal harvest date
Signal-to-noise ratio
Flesh color
Soluble solids content

ABSTRACT

Visible/near infrared spectroscopy (Vis-NIRS) was used to monitor the yellow-fleshed kiwifruit (*Actinidia chinensis* Planch 'Jintao') ripening on two selected orchards along 13 weeks, from pre-harvest to the late harvest. Calibration models for several Internal Quality Attibutes (IQA) were built from the spectral data of 375 individual kiwifruit. The analyzed IQA were L*, a* and b* from the CIELAB color space, hue angle, chroma, firmness, dry matter (DM), soluble solids content (SSC), juice pH and titratable acidity (TA). Different pre-processing methods were tested for the construction of PLS calibration models. SSC and Hue were the best performing models with a correlation coefficient of 0.81 and 0.88, and root mean square error of prediction (RMSEP) of 1.27% and 1.95°, respectively. The interpretation of the models in terms of the known absorption bands and the impact of signal to noise ratio (SNR) in them is discussed. The calibration models were used to perform average predictions of the IQA on orchard subareas, for each day of the experiment. These average predictions were compared with the IQA's average reference values on the same subareas and days. The model's metrics improved significantly through the averaging procedure, with RMSEP = 0.26–0.36% and $R^2 = 0.99$ for SSC; and RMSEP = 0.42° – 0.56° and $R^2 \approx 1$ for Hue. Since orchard management is done essentially through averages and not individual values, this result reinforces the applicability of the NIR technology for follow-up of fruit ripening in the tree.

1. Introduction

The assessment of the optimal harvest date (OHD) is fundamental for the quality, fruit management, storage time and disease liability (Berardinelli et al., 2019); if harvested too early, the fruit will not be able to properly ripen during storage and will develop poor flavor; on the other hand, if harvested too late, their storage ability will be reduced (Liu et al., 2019). Therefore, an appropriate harvest date for climacteric fruit ensures that the quality/flavor of fruit will be approved by the consumers, who have become more concerned about health and nutritional aspects. This is one of the reasons why kiwifruit is widely appreciated, not only for its flavor, but also for its vitamin C content (Beever et al., 1990), among other important nutritional characteristics.

Kiwifruit shows minor visual external changes, so that its appearance does not give any information about its maturity degree (Liu et al., 2019). For all kiwifruit species/cultivars, the major internal quality attributes (IQA) to determine harvest date are the soluble solids content (SSC), firmness and dry matter (DM). However, for the yellow-fleshed kiwifruit varieties which are more aromatic and sweeter than the green ones, and present a higher commercial value (Testolin and Ferguson, 2009), their unique flesh color has a major impact on the consumer (Schaare and Fraser, 2000). For that reason, it is also important to include the flesh Hue, to prevent still green-fleshed fruit to enter shelf-life. In fact, yellow fleshed cultivars are harvested when the Hue angle reaches the minimum of 103°, representing the flesh color changes from green to yellow (Costa et al., 2010).

The measurement of these ripening parameters is usually performed by fruit destructive methods, which are time consuming and do not allow to follow the same fruit over time. Furthermore, to avoid fruit and time waste, only a few samples are analyzed, which is not statistically representative of the entire biological variability, leading to a deficient harvest crop management (Cavaco et al., 2018).

The use of non-destructive methods for quality measurements plays an important role when determining the fruit ripening stage, since it

* Corresponding author at: CEOT, Universidade do Algarve, Campus de Gambelas, 8005-189 Faro, Portugal.
E-mail address: rguerra@ualg.pt (R. Guerra).

https://doi.org/10.1016/j.postharvbio.2022.111895
Received 2 August 2021; Received in revised form 26 February 2022; Accepted 27 February 2022
Available online 15 March 2022

allows for extensive monitoring of fruit in all conditions. Visible/ near infrared spectroscopy (Vis-NIRS) is a non-destructive, low-cost, flexible and reliable method that can be used to analyze multiple fruit quality attributes simultaneously (Nicolai et al., 2007; Cruz et al., 2021), and has been the principal choice for commercial applications (Walsh et al., 2020a). For completeness, it must be mentioned that other techniques are also used to monitor IQA: for SSC, dielectric spectroscopy (Ragni et al., 2012; Fazayeli et al., 2019), color and fluorescence imaging (Nie et al., 2020); for firmness, non-contact laser air-puff method (McGlone and Jordan, 2000), mechanical measurements (Ragni et al., 2010; Blanke, 2013; Pourkhak et al., 2017), acoustic method (Javadi and Nasiri, 2017) and dielectric spectroscopy (Ragni et al., 2012; Fazayeli et al., 2019); and for pH by dielectric spectroscopy (Fazayeli et al., 2019).

Regarding Vis-NIRS, there are already many published reports, which differ essentially by the coverage of the various sources of IQA variability. The IQA depend, in general, on the orchard, cultivar, year, weather conditions, cultural practices, ripening stage, cold storage (if used), shelf-life and even on the variability of fruit among trees and within the same tree (Musacchi and Serra, 2018; Cavaco et al., 2021). Therefore, it is important to mention and classify previous studies according to the source of variability they cover. This will allow to position this work relatively to the body of knowledge already produced in the area.

First of all, some published works concentrate merely in demonstrating the viability of Vis-NIRS to predict IQA. These studies use one homogeneous batch from a single orchard or local market and tend to deliver optimistic results due to the lack of variability in the dataset (Fu et al., 2007; Tang et al., 2010a, 2010b; Moghimi et al., 2010; Zhu et al., 2017; Benelli et al., 2021). A second group of publications still uses only one orchard, but gathers more variability by measuring fruit in different conditions, either by allowing some delay between the measurements or by using different storage and/or shelf-life conditions. This was done by Arazuri et al. (2005) and Shibang (2021). The work of Ciccoritti et al. (2019) added another layer of variability, by sampling the fruit in two successive years, while Guo et al. (2016) and Vieira et al. (2017) used two different harvesting dates to include fruit in different ripening stages.

Studying multiple orchards allows to include simultaneously several sources of variability (soil, weather conditions, cultural practices). For example, Lee et al. (2012) used data from three orchards and Sarkar et al. (2020) from ten different orchards and four cultivars. More complex datasets were obtained again by combining different orchards/origins and shelf-life conditions (Li et al., 2018) and even cold storage (McGlone et al., 2002; Lee et al., 2019; Guo et al., 2019). The study of Li et al. (2017) used data from three seasons. Very complete datasets were obtained by combining different orchards/origins and harvest times with different: *i)* shelf-life conditions (Schaare and Fraser, 2000); *ii)* storage conditions (McGlone et al., 2007); *c)* both shelf-life and storage conditions (McGlone and Kawano, 1998; Chen and Han, 2012). A general trend is that the broader is the range of variability included in the model, the lower is its predictive model accuracy.

Chemometrics are essential to extract relevant information from fruit spectral data that contain a large amount, complex and overlapping bands (Moghimi et al., 2010; Li et al., 2019), aside from the instrumental noise, scattering and ambient and other sources of variability that affect the spectra (Malegori et al., 2017). Chemometrics methods such as principal component analysis (PCA), principal component regression (PCR), and partial least square (PLS) are widely performed to enhance the calibration models' performance related to fruit quality (Mishra et al., 2021), being PLS the dominant technique used in relating fruit spectra to attributes (Walsh et al., 2020b) and used in its basic form in this work.

The objectives of this investigation were to simulate a real life situation of orchard monitoring, starting the measurement period as early, as two months before harvest, to late-harvest and to predict the average IQA of a set of fruit (harvested on the same day) to test whether average predictions could represent an improvement over individual ones and allow for an efficient follow-up of ripening. The motivation for this is that individual fruit IQA are not relevant for the management of an orchard, particularly to make the decision of harvesting, which is done by considering average values. Correspondingly, average predictions are of more interest than individual fruit predictions. Another goal was the construction of calibration models for 'Jintao', using data from two different orchards and a very complete set of IQA: L*, a* and b* from the CIELAB color space, hue angle, chroma, firmness, DM, SSC, juice pH and TA.

2. Materials and methods

2.1. Fruit

Yellow-fleshed kiwifruit (*Actinidia chinensis* Planch 'Jintao') were picked randomly from 25 tagged trees (one fruit/tree/sampling day) in two commercial orchards, namely, orchard 1 (41°39′23.6" N, 8°18′21.6" W, planted 2013) and orchard 2 (41°38′58.2" N, 8°18′26.0" W, planted 2014), located in Goães - Amares (Braga), Portugal (Fig. S1 of Supplementary Material). There is no distinction in edaphoclimatic or horticultural practices among the two orchards, which are described in more detail in the Supplementary Material.

Fruit sampling started two months before the commercial harvest season and ended at least one week after it (7 or 8 samplings, August 2018 - November 2018). After harvested, their temperature were determined with an infrared handheld digital thermometer EEM100 (Perel, Velleman, Belgium) and the Vis-NIR spectra acquired from each fruit. Each sampling was always performed in both orchards on the same day. Then, all fruit were shipped to the laboratory, where complementary standard destructive measurements were made in the next day. In total, 375 kiwifruit were collected and evaluated (200 orchard 1 + 175 orchard 2). The flowchart for sampling and measurement procedures is available in the Supplementary Material, Fig. S2.

2.2. Spectroscopy

The spectroscopy setup consisted of a Vis-NIR spectrometer USB4000 (Ocean Optics, USA), working in the range 345 – 1037 nm, a light source LS-1-LL (Ocean Optics, USA) and a bifurcated fiber with an interactance probe FCR-7UVIR400–2-BX/ME (Avantes, Holland). The probe works by sending light from the source to the sample through six illumination fibers and collecting the sample's reflection by a 7th fiber, in the center of the reflection probe, that is coupled to the spectrometer. The absolute reference material was a disk of Spectralon white surface (WS-1, Ocean Optics, USA), held at a constant height (0.47 mm) below the probe. The fruit to measure were introduced into a cup. The lid of the cup had a hole for the insertion of the probe and insured blocking of the sunlight during the spectroscopic measurements. This setup is very similar to the one described by Cavaco et al. (2018). The main difference was that three spectra were acquired along the equatorial area of each kiwifruit, in order to improve the measurements' statistics.

2.3. Fruit quality attributes

The several IQA were measured following a sequence. First, a 1 mm thick skin was removed at both opposite equatorial sides of kiwifruit for measurements of pulp firmness by puncture with a texturometer (Chatillon TCD200, Digital Force Gauge DFIS 50, John Chatillon & Sons, Inc., USA) using a cylinder probe of 8 mm at a depth of 7 mm and pulp color with a Minolta Chroma Meter CR-300 (Minolta, Japan) using the CIE L*a*b* space. The hue angle color (h°) was calculated by the equation $h^{\circ} = \arctan(b*/a*)$ and chroma by $C* = (a^{*2} + b^{*2})^{1/2}$ (McGuire, 1992). Then, 3 mm thick kiwifruit equatorial slices (1 per fruit) were cut,

weighed and then dried at 105 °C until constant weight for determination of DM, expressed as percentage of dry weight relatively to fresh weight (%). The remaining of the kiwifruit were peeled and squeezed. The juice filtered by a cotton cloth was used for the measurements of SSC, pH and titratable acidity (TA). SSC was determined by using a digital refractometer HI 96801 (Hanna Instruments, USA) and expressed as %. With a TitroLine 6000 (SI Analytics, Germany), juice pH and Total TA, expressed as mass percentage of citric acid per 100 mL juice (%), were determined using 2 mL kiwifruit juice diluted with 8 mL distilled water titrated with 0,1 N NaOH until a pH of 8.2.

2.4. Data analysis

The descriptive statistical analysis of the IQA was performed in IBM SPSS Statistics 27 (IBM Corp., Armonk, NY, USA). The nonparametric multivariate Kruskal-Wallis (MKW) test was used to compare the dependent variables in each orchard. The effects of orchard and date on each of the quality parameters were tested by a full factorial MANOVA (type III) and further multi-comparisons among variables were performed by the Bonferroni test for a significance level of $p < 0.05$. (Oja, 2010).

The multivariate data analysis were performed in MATLAB R2019a, version 9.6 (The MathWorks, Inc., Natick, MA, USA). The PLS1 regression was calculated through the NIPALS algorithm, available, for example, in Andersson (2009). The Savitzky-Golay filter (Savitzky and Golay, 1964) was implemented through the function *savgol* of the PLS Toolbox (PLS Toolbox, version 8.7, Eigenvector Research, Inc., Manson, WA, USA). The VIP scores were calculated as explained in Farres et al. (2015).

2.5. Spectroscopic signal to noise ratio

The signal-to-noise ratio (SNR) calculation was performed on R, the reflectance matrix. Each line of R is a spectrum $R_i(\lambda)$ ($i = 1, \ldots, M$ = number of fruit). The following steps were taken: 1) Smoothing of each line of R by a Savitzky-Golay filter (denoted SG(width, order)) of 81 points and second polynomial order, $S_i(\lambda) = SG(R_i(\lambda), 81, 2)$. 2) Calculation of the squared fluctuations (around the baseline) for each spectrum: $F_i^2(\lambda) = (R_i(\lambda) - S_i(\lambda))^2$. 3) The noise level at each wavelength was calculated by assuming that the fluctuations on the 40 closest neighbors are equivalent to those that would be observed in 40 repetitions at the same wavelength (time fluctuations) as $n_i(\lambda) = \sqrt{SG(F_i^2(\lambda), 41, 0)}$. 4) SNR for each spectrum was calculated by $SNR_i(\lambda) = S_i(\lambda)/n_i(\lambda)$. 5) The final noise figure was calculated from the average of all fruit: $SNR(\lambda) = \sum_i SNR_i(\lambda)/M$.

2.5.1. Pre-processing

Pre-processing included three different procedures: elimination of hot pixels, transformations and elimination of outliers. Hot pixels were identified visually and their counts substituted by the mean value of the two adjacent pixels. The transformations of spectra used were absorbance ($\log(1/R)$), standard normal variate transformation (SNV) (Barnes et al., 1989) and the Savitzky-Golay filter (Savitzky and Golay, 1964), either for smoothing or derivation (first and second derivatives). Combinations of these transformations were also performed. The spectral range was also tested, from the full spectrometer range, 345 – 1037 nm, to subranges obtained by varying systematically the upper and lower limits. Outlier samples were detected and rejected. Three types of outliers were considered: *i)* when the norm of the transformed spectra diverges from the average norm more than 3 standard deviations (3σ outliers); *ii)* 3σ outliers in the PLS scores of the calibration samples; *iii)* 3σ outliers in the PLS projected scores of the validation samples.

2.5.2. Calibration models

Calibration models were obtained for the following IQA: L*, a* and b* from the CIELAB color space, hue angle, chroma, firmness (N), dry matter % (W/W), soluble solids content (%), juice pH and titratable acidity (%). Data modeling was performed in two ways. The first approach was the usual development of calibration models for the various IQA and subsequent validation on independent individual fruit. The second approach was to use those models to perform the prediction of average IQA for each orchard and each day.

Partial Least Squares (PLS) models were obtained using all data from both orchards and from all measurement days. Data from each orchard was divided in 2 subsets according to the number of the tagged tree (trees 1–12 assigned to the first subset and trees 13–25 to the second subset). The whole data was subjected to a 4 × 5-fold double (or nested) cross validation (CV). The pseudo-code described in Filzmoser et al. (2009) has been implemented, except that there was no repetition (a single run was performed).

- Each segment ($i = 1, 2, 3, 4$) is taken at a time as test set, and the remaining three aggregated as calibration set (outer loop).
- CV is performed in each calibration set i. First, it is divided in 5 splits (Venetian blinds, in this work). Then, each split ($j = 1, 2, 3, 4, 5$) is taken at a time as validation set and the remaining four are aggregated as training set (inner loop). The optimal number of latent variables, $nLV_{opt}(i)$ is obtained and the corresponding PLS model built from the entire calibration set i.
- The i-th PLS model is applied to the i-th test set.
- A global statistic is calculated from the four test sets.

The nomenclature is taken from Filzmoser et al. (2009): calibration/test sets for the outer loop, training/validation sets for the inner loop. A graphical illustration is presented in Supplementary Material, Fig. S3. The performance of the models was characterized by the parameters (Nicolai et al., 2007): root mean square of error in prediction (RMSEP), the squared correlation coefficient (R^2), the standard deviation ratio (SDR), the bias and the slope. For completeness, the definitions are provided in the Supplementary Material.

The average and standard deviation of the reference IQA values and their corresponding predictions were calculated for each day and orchard, resulting in a dataset of 8(7) pairs of values (average prediction, average reference value) for orchard 1(2). The prediction statistics were calculated from these pairs of values, specifically, RMSEP, R^2, bias and SDR. Furthermore, the average predictions were compared with the average reference measurements through a t-test.

3. Results and discussion

3.1. Temporal evolution of the average spectra and its relation with tissue structure

The time evolution of the spectra has a similar coarse pattern (Figs. 1A and B). The first three days have higher NIR plateaus, in the range 50–70%, while the last days have diminished plateaus, in the level 35–50%. One of the main factors explaining the variation in the plateaus' height is the fruit firmness. It is usually assumed that flesh firmness is diretly related with the scattering coefficient and that higher firmness implies more backscattering and a higher level of reflectance. There is indeed a loose relation between the plateau height (measured by the representative wavelength of 842 nm) and the firmness (Fig. 1D), observed as a global trend of increase in reflectance with firmness, but with a large variability superimposed. This means that there are more factors needed to explain the height of the reflectance plateau than the firmness alone.

In the context of ripening follow-up it is important to understand the causes of the decrease in the NIR plateau, since it signals an internal change in fruit. However, the relationship between the reflectance spectra and the fundamental structural and mechanical properties (such as firmness) of plant material (Cen et al., 2013) is not well established,

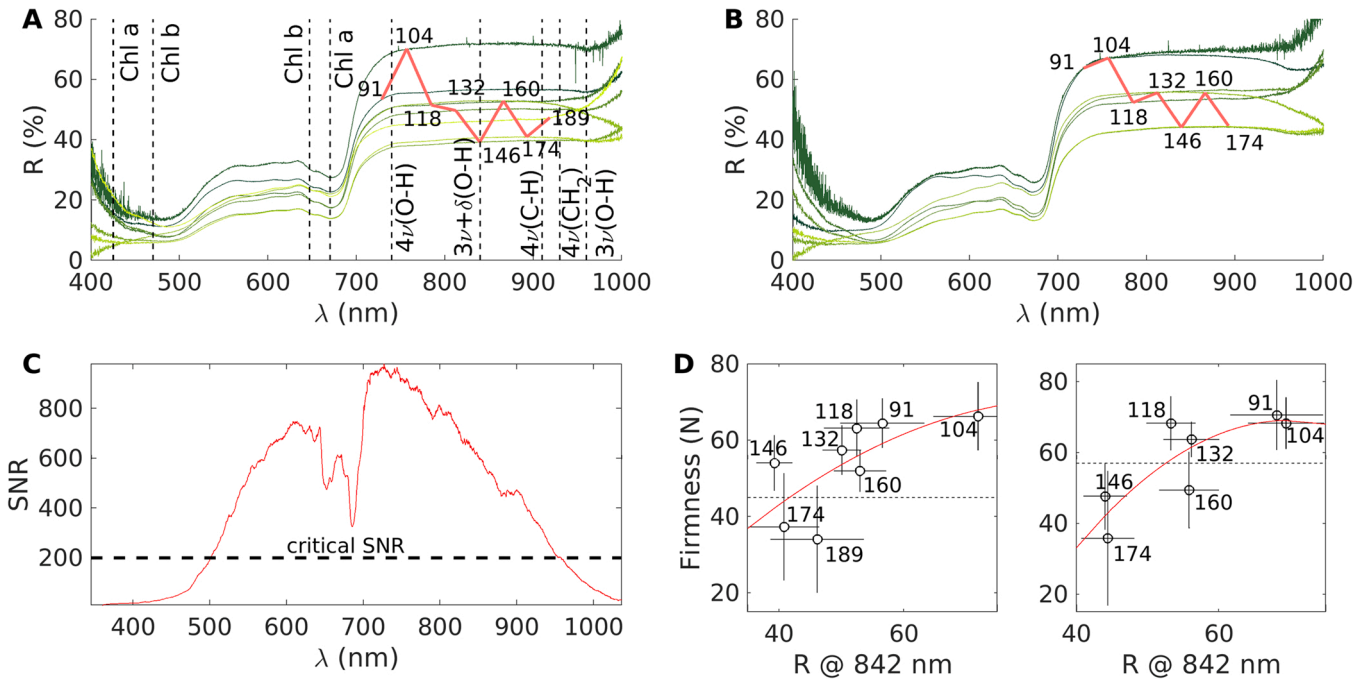

Fig. 1. (A and B) Daily average of Vis-NIR kiwifruit reflectance spectra acquired along time, for orchards 1 and 2, respectively. The numbers above the NIR plateaus indicate the days after full bloom (DAFB). The lines in A represent the nominal positions of the main absorption bands, identified by the overtone (n indicates the (n-1)-th overtone) and the type of oscillation (ν for stretching and δ for bending). C) Spectrometer signal-to-noise ratio (SNR) as a function of wavelength. D) Relation between the reflectance at 842 nm, R@842 nm, and the firmness for orchard 1 (A) and orchard 2 (B). The numbers represent the measurement day, the horizontal bars represent the standard deviation of R@842 nm and the vertical bars represent the standard deviation of firmness.

since light interaction with turbid biological materials is a complicated phenomenon, involving both absorption and scattering (Qin and Lu, 2008), whose effects can not be separated (Cen et al., 2013). Light absorption is related to tissue's chemical composition, while scattering is influenced by physical and structural properties, such as firmness and cell size (Cen et al., 2013; Cheng et al., 2019). However, the height of the reflectance plateau can not be taken as a direct measure of firmness, since the scattering effect it represents is always coupled with the absorption effect.

Summarizing, *i)* there was an average trend of decrease in the NIR plateau accompanying the ripening process, but *ii)* there was a large variability in that trend, which means that the relationship between firmness and the NIR plateau is not simple Table 1.

3.2. Spectroscopic signal to noise ratio

SNR drops below 500 nm and above 950 nm (Fig. 1C). This is due to the quantum efficiency of the detector, but it is further shaped by the absorption of pigments, specifically below 450 nm and around 680 nm. The two valleys at 640 and 680 nm correspond to the red absorption peaks of chlorophyll *b* and *a*, respectively. These valleys are not clearly identified in the reflectance curves, suggesting that SNR analysis may provide a way to increase the spectral resolution. The water peak around 960 nm falls partly outside the ideal range, that should thus be approximately 500–950 nm, which compromised its usefulness for model calibration. The construction of calibration models employed the whole spectroscopic available range and the systematic test of sub-ranges. The selection of optimal ranges coincided, in most cases, with the spectral range insuring SNR> 200 (Table 2), suggesting that the SNR criteria may even have precedence over the information criteria for the construction of models. The DM model is a clear demonstration of this fact, since it excludes the water band.

3.3. IQA temporal evolution

The initial averages of SSC, Hue and firmness for orchard 1 were respectively 4.5%, 117.3 °Hue and 64.5 N, while their final values were 11.5%, 104.5 °Hue and 34.8 N. For orchard 2 the corresponding values were 11.5%, 104.5 °Hue and 34.8 N in the beginning and 12.4%, 100.3 °Hue and 35.8 N in the end (Table S7 and Figs. S4–S7 in Supplementary

Table 1
Global descriptive statistics of the Internal Quality Attributes (IQA) in the two orchards.

	Orchard 1			Orchard 2		
IQA	mean ± std	max	min	mean ± std	max	min
SSC	6.9 ± 3.1	17.3	3.5	7.0 ± 3.0	16.2	3.7
Firmness	53.6 ± 14.6	84.3	1.7	57.7 ± 16.3	91.9	2.2
Dry matter	14.1 ± 2.0	19.4	9.6	14.5 ± 2.0	18.7	10.3
TA	1.18 ± 0.12	1.66	0.88	1.07 ± 0.13	1.44	0.50
pH	3.22 ± 0.19	3.78	2.78	3.14 ± 0.14	3.60	2.85
L*	62.8 ± 4.2	74.5	48.4	64.7 ± 4.1	74.0	53.0
a*	− 13.3 ± 3.4	-3.8	-17.7	− 12.4 ± 3.8	-4.7	-17.5
b*	− 31.9 ± 2.2	39.5	23.3	32.7 ± 2.3	39.9	26.1
Hue	112.5 ± 5.2	118.0	96.7	110.7 ± 6.3	118.0	97.9
Chroma	34.7 ± 2.6	40.9	23.9	35.2 ± 2.2	40.5	27.7

Table 2
Summary of principal results obtained in the PLS models for each quality attribute.

IQA	RMSEP	R^2	SDR	Bias	Slope	Range	Preproc
SSC	1.27	0.81	2.31	-0.10	0.80	675–895	SNV
Firmness	9.47	0.57	1.5	0.81	0.56	635–870	SNV
Dry matter	1.19	0.65	1.69	0.03	0.68	595–931	SNV
TA	0.12	0.19	1.13	0.00	0.24	809–883	SNV
pH	0.12	0.45	1.34	0.00	0.50	470–948	SNV
L*	2.84	0.48	1.38	0.11	0.52	470–840	SNV
a*	1.35	0.85	2.60	-0.05	0.86	660–948	SNV
b*	1.64	0.32	1.21	0.13	0.33	470–660	SG+ SNV
Hue	1.95	0.88	2.92	0.15	0.86	660–959	SNV
Chroma	1.71	0.27	1.17	0.09	0.31	486–660	SG+ SNV

Material).

The Hue values showed an initial plateau but, as expected, they decreased along time, for both orchards. Relatively to the inter-orchard comparison, the values for orchard 2 were always lower than those for orchard 1, with the exception of first date. In fact, the kiwifruit from orchard 2 became yellow-fleshed sooner and reached the color criteria needed for the harvest 160 DAFB (Table S7). Usually, kiwifruit are harvested after reaching, on average, minimum values of 6.5% SSC and flesh hue angle 103°. The Hue histograms (Fig. S4, B and C) show a dominant bar around 115°, corresponding to the initial plateau encompassing the first three data acquisitions (91, 104 and 118 DAFB).

Firmness showed also an initial plateau (91, 104, 118 and 132 DAFB) and then decreased for both orchards. Firmness was higher in orchard 2 in three of the four first acquisition days (91, 104 and 118 DAFB). In the end, the firmness values from the two orchards were equal. Overall, orchard 1 ripened progressively throughout time, while orchard 2 was more irregular. There was also a clear peak in the histograms, around 60 N, linked to the same initial plateau mentioned above (Fig. S5, B and C).

The temporal evolution of SSC showed also an initial plateau, corresponding to that of firmness (91,104, 118 and 132 DAFB), but is more flat. In this plateau the SSC values were very similar in both orchards and around 5%. This explains why the SSC histograms (Fig. S6, B and C) are the more asymmetrical of the four IQA's analyzed, with huge peaks at 5%. After the 5% plateau, on the fifth acquisition date (146 DAFB), the SSC rise very fast, although much more intensely on orchard 2 (average values on 146 DAFB $>$ 8%) than in orchard 1 (average $<$ 6%). Overall, orchard 1 had a more smooth evolution curve, as was also the case in firmness. As in Hue, orchard 2 reached sooner the stipulated SSC to be harvested and stored.

Contrary to the other three IQA, DM did not show an initial plateau. DM values increased from the first date onward. This is a direct result of fruit growth and development, which comprise the enlargement of many pulp tissues, such as cell expansion, cell wall thickening and starch accumulation (Schroder and Atkinson, 2006). Without the initial plateau found in the other IQA, the DM histograms (Fig. S7, B and C) bear more resemblance with a normal distribution than the previous ones. DM is also the only IQA showing a tendency to peak before the end of observations.

Despite the two orchards were on the same region with similar cultural practices, their specific location seem to affect the fruit ripening (Cavaco et al., 2021). In fact, the orchard 2 harvest started 167 DAFB, while in orchard 1 it was initiated one week later. The different timings exhibited by them demonstrate the importance of assessing the major ripening attributes of 'Jintao' kiwifruit along time and in each orchard, to establish more precisely the optimal harvest date at each site and therefore provide fruit with better quality to consumers.

3.4. Calibration models for the IQA

3.4.1. SSC

A previous remark valid for all the IQA calibration models is that their wavelength ranges were always shortened relatively to the full range available, either in the lower and in upper values. The main reason to eliminate the upper wavelength region is the noise due to low quantum efficiency of the detector and corresponding low SNR (especially above 950 nm). The main reason for the elimination of lower wavelength regions is that the chlorophyll dominated band is not always useful as a predictor for other attributes.

The model SSC model delivers good performance in the context of Vis-NIRS in fruit (Fig. 2A and Table 2). However, a closer inspection reveals that the predictions saturate around 12% SSC. This does not correspond to the upper range of the SSC values, since the reference measurements include fruit up to 16% SSC. But the model predictions breaks in the upper SSC range (12–16%) because of the small number of fruit in this range (cf. Fig. S6, B–C). This is particularly clear for the test set #3 (circles). The descriptive statistics of the four test sets may be read from Table S2 in the Supplementary Material. Test set #3 has a maximum SSC of 16.2%, which exceeds by more than 1% the maximum value in calibration (15.1%). Therefore, the larger deviations from the measured values in Fig. 2A are observed mainly in the circles.

With RMSEP = 1.27%, the current results are within the same order of magnitude of those from Benelli et al. (2021) [0.73–1.10%], Clark et al. (2004) [0.76–0.92% in IV], Guo et al. (2019) [0.9%], Lee et al. (2019) [1.38–1.58%], Li et al. (2017) [0.66–1.02%], McGlone and Kawano (1998) [0.47–0.96% in EV], Sarkar et al. (2020) [1.0–2.1%] and Vieira et al. (2017) [1.0%].

The VIP scores (Fig. 2B) indicate that the SSC model is relying mostly

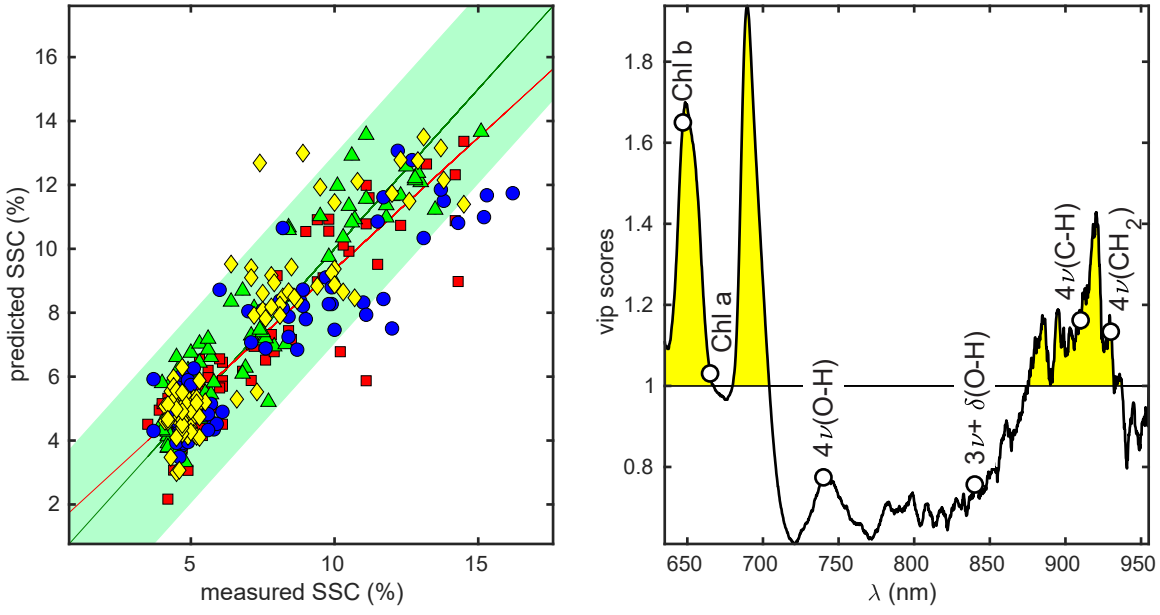

Fig. 2. A: measured versus predicted values for kiwifruit SSC. Each symbol corresponds to one test set. The green shadowed band has a half-width equal to the standard deviation of SSC. B: average VIP scores of the four models. The shadowed area corresponds to VIP $>$ 1 and the white circles to the nominal position of the spectroscopic bands indicated.

on the chlorophyll band and on the third overtone of CH and CH_2 stretching, usually assigned to 910 – 930 nm. These three VIP bands illustrate the three main sources of information for the calibration models in Vis-NIRS. The chlorophyll band around 680 – 690 nm represents an indirect source of information. Indeed, chlorophyll degradation and SSC are inversely related along ripening. Thus, chlorophyll content is a proxy for SSC but not a direct measure of it. But the 4ν(C–H) and 4ν (CH_2) bands are direct sources of information, since they relate directly with the concentration of organic molecules and may reflect changes in the sugar content. An interesting detail is the peak associated with the band 4ν(O–H). It is below the level VIP= 1, but still is recognized by the model as locally relevant.

SSC models are the most frequent in the literature and therefore their discussion covers most of the relevant comments for comparison between published results and associated methods. A mandatory precautionary note is that there are no SSC models for 'Jintao', except that of (Vieira et al., 2017) [although there is extensive experience with the Kiwi Meter (Rocchi et al., 2016), it does not provide directly SSC]. Of course, the results obtained in other kiwifruit cultivars are relevant for the comparison. And it turns out that the results of SSC model developed this work are inferior to most the results published in the literature.

The global panorama of the published models may be understood by two main factors: *i)* the quality of the equipment, which translates in SNR values across some wavelength range; *ii)* the fruit variability covered in the dataset (different orchards or sources, harvesting periods, shelf-life and storage conditions). And there is a third, transversal factor to explain the performance parameters, which is the use of a proper external validation (EV). In the following paragraphs these factors are discussed, together with other secondary features that may add additional insight into the results. Results from other authors are quoted in the text and are available in the Supplementary Materials, in Tables S5–S6, for ease of comparison.

The large majority of the published studies use internal validation (IV), which used an homogeneous splitting of the entire dataset as calibration and validation, while in EV, calibration and validation are heterogeneous datasets, obtained, for example, from different orchards or years. EV is more demanding than IV and therefore, a degradation of the results is expected when going from IV to EV. Examples of that difficulty may be found in McGlone and Kawano (1998) [RMSEP ~ 0.4% in IV vs. RMSEP ~ 0.5 – 1% in EV]; in Clark et al. (2004) [RMSEP ~ 0.8 – 0.9% in IV vs. RMSEP ~ 1.4% in EV] and Li et al. (2018) [RMSEP ~ 0.8%]. Taking into account that the present work used IV, the SSC model performance (RMSEP = 1.27%) resembles more that of EV results. The 4 × 5-fold double cross validation method used here increased RMSEP only by 0.1% relatively to the standard IV (results not shown), so that other factors should explain the large RMSEP obtained.

There is a clear trend in the published reports: the more homogeneous the dataset, the better the predictions for SSC. For example, Moghimi et al. (2010) [RMSEP = 0.32%], Zhu et al. (2017) [RMSEP = 0.4%] or Shibang (2021) [RMSEP = 0.36%] use only one source/orchard and limited size datasets. Adding more variability by measuring fruit in different conditions, either by allowing some delay between the measurements or by using different storage and/or shelf-life conditions, usually tends to increase RMSEP. For example, Arazuri et al. (2005) included five different conditions in shel-life and obtained RMSEP ~ 0.7% (average of results in that paper). Guo et al. (2016) acquired two lots separated two weeks and measured the fruit in several days, along ripening, obtaining RMSEP ~ 0.6 – 1.0%. Models with several orchards tend to deliver the higher (and more realistic) RMSEP values. For example, Clark et al. (2004), with 20 orchards obtained RMSEP ~ 0.8 – 0.9% (in IV); Li et al. (2017), with 50 orchards obtained RMSEP ~ 0.7 – 1.0%; Lee et al. (2019), with 3 orchards obtained RMSEP ~ 1.4 – 1.6%: and Sarkar et al. (2020), with 10 orchards obtained RMSEP ~ 1.0 – 2.1%.

The present work adds a new source of variability to the data. For the first time, the data includes measurements from the early pre-harvest. In the previous studies the variability is obtained by collecting the fruit some weeks before or after the harvest (commercial season) or by changing postharvest conditions. In this work, the variability is obtained from the very ripening process, along a period of 12 (orchard 2) or 13 weeks (orchard 1). Therefore, the data sets were very heterogeneous, including fruit in very different developmental stages. This means very different chemical and structural compositions mixed in the same data set. For example, the proportion of starch and sugars is very different at harvest and 10 weeks before, which represents an additional difficulty for retrieving information from the C–H bands. And the cellular structure also changes considerably in that period, introducing more variability in the scattering effects. These factors necessarily sum up to degrade the calibration models' performance obtained in this work when compared to others developed more homogeneous samples.

The spectrometer used in this work is noise limited above 950 nm, due to very poor SNR (Fig. 1C). For this reason, important bands might be not included in the models. For example, the water band at 960 nm, 3ν(O–H), should have an indirect, but important role in the SSC model (since more solubilized solids mean less absolute quantity of water per juice unit volume). However, the best model for SSC did not include it, probably because of low SNR in that band. Therefore, low SNR in the water band may degrade the model predictions and this applies to all the models developed in this work.

3.4.2. Colorimetric parameters

The Hue pulp calibration model also delivers good performance (Fig. 3A and Table 2). There is an agglomeration of points in the upper part of the plot because the majority of the fruit had Hue above 110°. However, a good linearity was maintained for the lower values of Hue.

There are not many reports on the prediction of Hue. Clark et al. (2004) obtained RMSEP = 0.85–1.37° in IV and 1.11° in EV, McGlone et al. (2007) obtained RMSEP = 0.98–1.05° and Schaare and Fraser (2000) obtained RMSEP = 1.63°. Again, the present results are inferior to the published ones, although similar to last one. A likely reason for that is the best SNR provided by the spectrometer employed by these authors, which allowed them to use lower wavelengths (Table S5).

The VIP scores plot has a prominent peak at about 660 nm (Fig. 3B), which may be assigned to the red peak of Chl *b*. Generally, there is a preponderance of the chlorophylls, *a* and *b*, in the model. Their importance is twofold: on one side there is an indirect correlation, since the chlorophyll content decreases simultaneously with Hue along ripening. On the other side, there is a direct correlation with the red color and thus with Hue. As in the SSC model, there are two more bands with VIP > 1, and they are the same: 4ν (O–H) and 4ν (C–H). These can not be a direct source of color information, since they are out of the visible. So, they are conveying indirect information, since the water and organic molecules content change along ripening.

Hue is a colorimetric parameter that changes approximately from around 120° (light green) to 100° (yellow-green) along the ripening process. Therefore, it would be expectable to have the best calibration model defined in the visible range or, at least, including green and yellow. However, this was not observed. Including the wavelength range below 660 nm (red) degraded the model. Part of the explanation is that the spectral range below 500 nm in the higher noise regime (Fig. 1C). Thus, the spectral band 400–500 nm is not included in the model. However, this does not explain why the band 500–660 nm is also rejected. This is probably due to the fact that absorption in that range is largely determined by carotenoid content, which changes much less than chlorophyll along ripening. Therefore the later relates much better than the former with changes in pulp color.

Skin color necessarily interferes with the pulp color measurement, since light must cross the skin twice, along the path between the light injection fiber and the light collection fibers. Furthermore, in the reflectance mode there are additional photons scattered by the skin, which are devoid of information from the pulp. As mentioned above, the interactance probe used in this work may have collected such photons

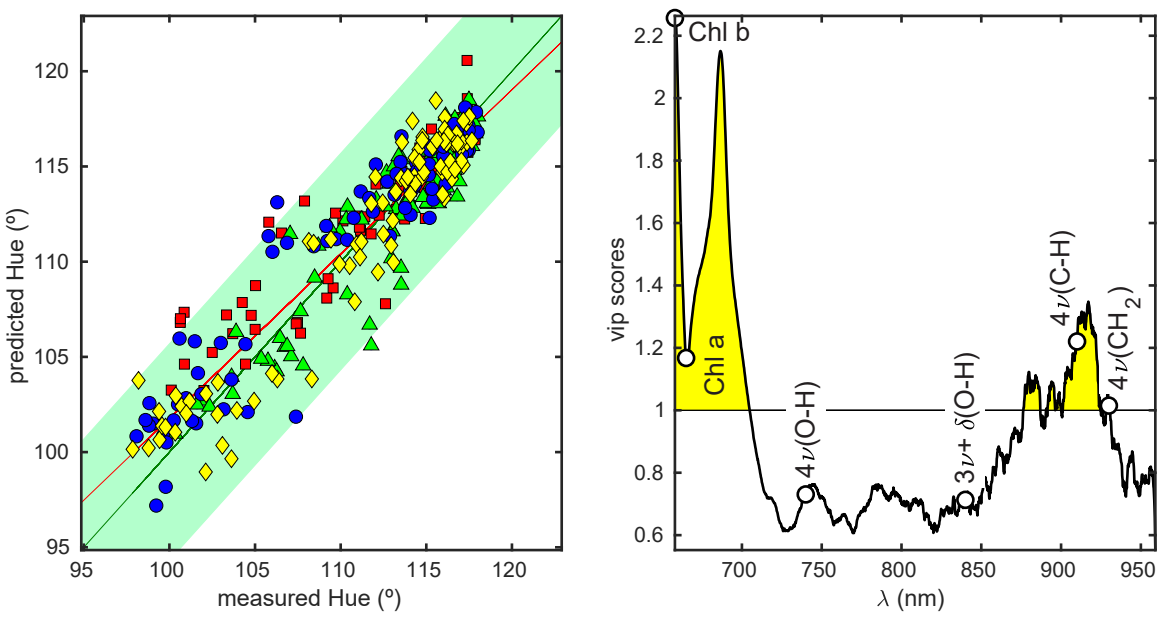

Fig. 3. A: measured versus predicted values for kiwifruit Hue. Each symbol corresponds to one test set. The green shadowed band has a half-width equal to the standard deviation of Hue. B: average VIP scores of the four models. The shadowed area corresponds to VIP > 1 and the white circles to the nominal position of the spectroscopic bands indicated.

with corresponding degradation of the results. On the other side, the near infrared part of the spectrum is less contaminated by the skin absorption because its pigments absorb essentially in the visible, and this explains why the calibration model includes the infrared.

Relatively to the other colorimetric parameters models, only a* delivers good performance (Table 2). Its VIP scores plot (not shown) reveal that the fundamental source of information is the chlorophyll band, with a minor contribution from the 4ν (C–H) band. This is in agreement with the fact that the a* measures the green to red transition and is intimately related with the chlorophyll content.

The performance of the remaining colorimetric parameters – L*, b* and Chroma – are all poor, with SDR < 1.4 for all the three cases. The poor performance of the b* model results from the difficulty in retrieving reliable information on the blue, as mentioned above. The average reflectance in the blue, although low, seems enough for the purpose of building models (Figs. 1A–B). However, SNR is very low in the blue (Fig. 2C) yielding a poor quality signal in that range and consequently a poor model. This finding highlights again the crucial role of SNR for obtaining good models. The difficulties found in the L* and Chroma models result from the original problems in the determination of b*, since the correct calculation of L* and Chroma depends on the correct estimate of b*.

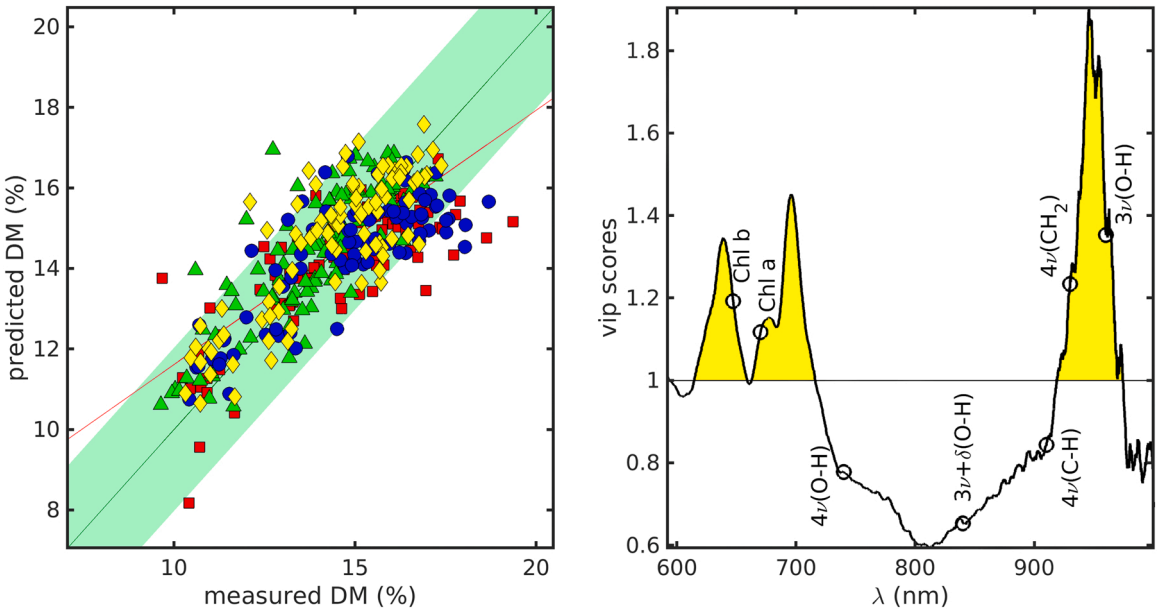

Fig. 4. A: measured versus predicted values for kiwifruit DM. Each symbol corresponds to one test set. The green shadowed band has a half-width equal to the standard deviation of DM. B: average VIP scores of the four models. The shadowed area corresponds to VIP > 1 and the white circles to the nominal position of the spectroscopic bands indicated.

3.4.3. Dry matter

The performance of the DM model is fair (Table 2). This means that coarse separation of fruit is possible, in high and low values. The comparison with the literature results is the most unfavorable of all the IQA. Published results for DM include RMSEP= 0.33% (Ciccoritti et al., 2019), 0.44–0.50% in IV and 0.54% in EV (Clark et al., 2004), 0.77% (Kim et al., 2018), 0.36–0.44% in IV and 0.47–0.69% in EV (McGlone and Kawano, 1998), 0.29% (McGlone et al., 2002), 0.24–0.40% (McGlone et al., 2007), 0.53–0.59% (Tang et al., 2010b), 0.41–0.57% (Tang et al., 2010a) and 0.73% (Vieira et al., 2017).

The results displayed in Table 2 are from the best models. For DM, the upper wavelength range is 931 nm, which excludes the main water peak. However, the result displayed in Fig. 4 shows another, sub-optimal model, that includes the water band. The reason to illustrate two different models is to discuss the role of the 3ν(O–H) absorption band, located near 960 nm. This is the main feature related to water content and yet the best model for DM (Table 2) did not include it. On the other side, the sub-optimal model of Fig. 4 includes the water band, which takes the prominent role, as observed in the VIP scores plot. Spectrometer noise is again the most likely explanation for the absence of the water peak in the best model, since the band at 960 – 980 nm is already in the higher noise regime (Fig. 1C). Since the changes in DM content are of the order of few percent (Table S7), a level of SNR below 200 (observed in the water band) makes a real difference in terms of numerical reliability. This is an extreme example of the importance of SNR, since the most important source of information was excluded due to the noise affecting it.

3.4.4. TA

The model for TA has poor to zero performance. With $R^2 = 0.19$, RMSEP= 0.12% and SDR= 1.1 it has an almost null predictive power (Table 2). It is interesting that the model of Vieira et al. (2017) predicted slightly better ($R^2 = 0.52$, RMSEP= 0.25% and SDR = 1.4), probably because it included wavelengths up to 1147 nm. The spectral range seems decisive here. Using an upper range of 2500 nm, Ciccoritti et al. (2019) and Lee et al. (2012) obtained $R^2 > 0.9$.

3.4.5. pH

The same comments of TA apply to pH, although the pH results are slightly better ($R^2 = 0.45$, RMSEP= 0.12 and SDR= 1.3). These are clearly worse than the two references available. Moghimi et al. (2010) obtained $R^2 = 0.94$, RMSEP= 0.076 and SDR= 2.6 in the range 400 – 1000 nm, while Zhu et al. (2017) obtained $R^2 = 0.91$, RMSEP= 0.015 and SDR= 2.6 in the range 951 – 1670 nm. However, in the former the number of samples was very limited and the spectrometer was a high-quality benchtop instrument, while the latter also used a limited number of samples, but may have benefited from a more adequate wavelength range.

3.4.6. Firmness

The calibration model of firmness has $R^2 = 0.57$, RMSEP= 9.47 N and SDR= 1.5, which means that it captures some information. Despite the moderate/poor result, the firmness model is the one that compares better with the literature, being approximately equal to those obtained by Benelli et al. (2021) [RMSEP= 9.9–14.5 N], Fu et al. (2007) [6.3–7.0 N], Li et al. (2018) [11.9 N], McGlone and Kawano (1998) [4.5–7.8 N in IV], Vieira et al. (2017) [11.6 N], although inferior to the results obtained by Lee et al. (2012) [2.8–4.0 N] and Li et al. (2017) [2.7–4.3 N]. The latter were obtained in the approximate range 400–2500 nm, which may point to some advantage of using longer wavelengths.

Inspection of VIP scores (data not shown) reveals again a preponderance of the chlorophyll band and some weight attributed to a new band centered around 785 nm. The relation with chlorophyll is indirect, as its content decreases together with firmness along ripening. On the other side, the 785 nm region is interesting in that it lacks relevant chemical absorption bands. However, this may be appropriate for modeling firmness, since the changes induced by the scattering effects of the tissue structure are less obscured by absorption effects in this spectral region.

3.5. Follow-up of kiwifruit ripening through predictions of the IQA averages at specific dates

The average daily measurements for Hue are very close to the average daily predictions (Fig. 5). And the same is true for SSC (Fig. 6). This is confirmed by the low number of asterisks in both figures, which signal different averages ($p < 0.05$). From the thirty data pairs shown in both Figs. 5A–B and 6A–B, only in six a statistically significant difference was found between prediction and real measurement. This translates into very high values of SDR in Figs. 5C–D and 6C–D. Indeed, any of the four SDR values shown is above 8 and three of them are above 10. The remaining parameters correspond equally to an excellent performance, e.g., $R^2 \sim 1$ and RMSEP values around 3–5 times lower than those obtained for individual predictions (Table 2, and Figs. 2 and 3).

There are a total of 150 mean values observed [(8 +7) days x 2 orchards x 10 IQA]. Of the corresponding 150 predicted mean values, only 12 (8%) are different from the observed mean values. This percentage is lower considering orchard 1 only (ca. 4%, or 3 in 80), but it is higher in orchard 2 (ca. 13%, or in 9 in 70). A detailed table of the 150 comparisons between measured and predicted averages is provided in Table S3 of the Supplementary Material. This is an excellent result, especially taking into account that the performance of some models is poor (Table 2). The conclusion is that the prediction of the average IQA for an orchard, or part of an orchard, is much more reliable than the prediction of individual IQA values. This was to expect, due to the averaging effect.

Therefore, good calibration models allowed to achieve excellent average models, which in turn allowed for an efficient follow-up of ripening in the orchard. Average predictions provide a very reliable way of monitoring ripening and predict the harvest date. For example, the average prediction of SSC in 160 DAFB signals perfectly the onset of harvesting in orchard 1 (Fig. 6A). For orchard 2, the average prediction at 146 DAFB is slightly delayed (Fig. 6B). In practice, more frequent assessments will allow to identify the IQA evolution patterns and to predict the optimal harvest date with some days/weeks in advance.

But why are poor models able to deliver good average predictions? Because the average values of the corresponding IQA vary very little from day to day. In other words, the averages to predict are approximately constant along ripening. This also implies that those IQA are useless for monitoring purposes (see Section S4 of the Supplementary Material).

4. Conclusions

The calibration models developed in this work were based on a very heterogeneous dataset, including fruit in very different developmental stages, from very unripe to overripe. Good models were obtained for Hue, SSC and a* . The experimental design allowed to test the accuracy of average predictions from these calibration models, specifically, to predict the average IQA for each of the sampling days and each of the four data subsets considered. The prediction of IQA averages at these specific dates revealed excellent results. As orchard management is done essentially through averages and not individual values, this result reinforces the applicability of the NIR technology in the field.

Regarding the limitations of this work, the following points must be borne in mind: 1. The total number of 375 fruit is still limited and the proof of concept results shown in this report must be subjected to more stringent validation, with fruit from another year. 2. This work used an internal validation scheme, and the average prediction concept must be challenged by an external validation scheme to demonstrate its robustness.

Future work will address these issues and also the reliability of the

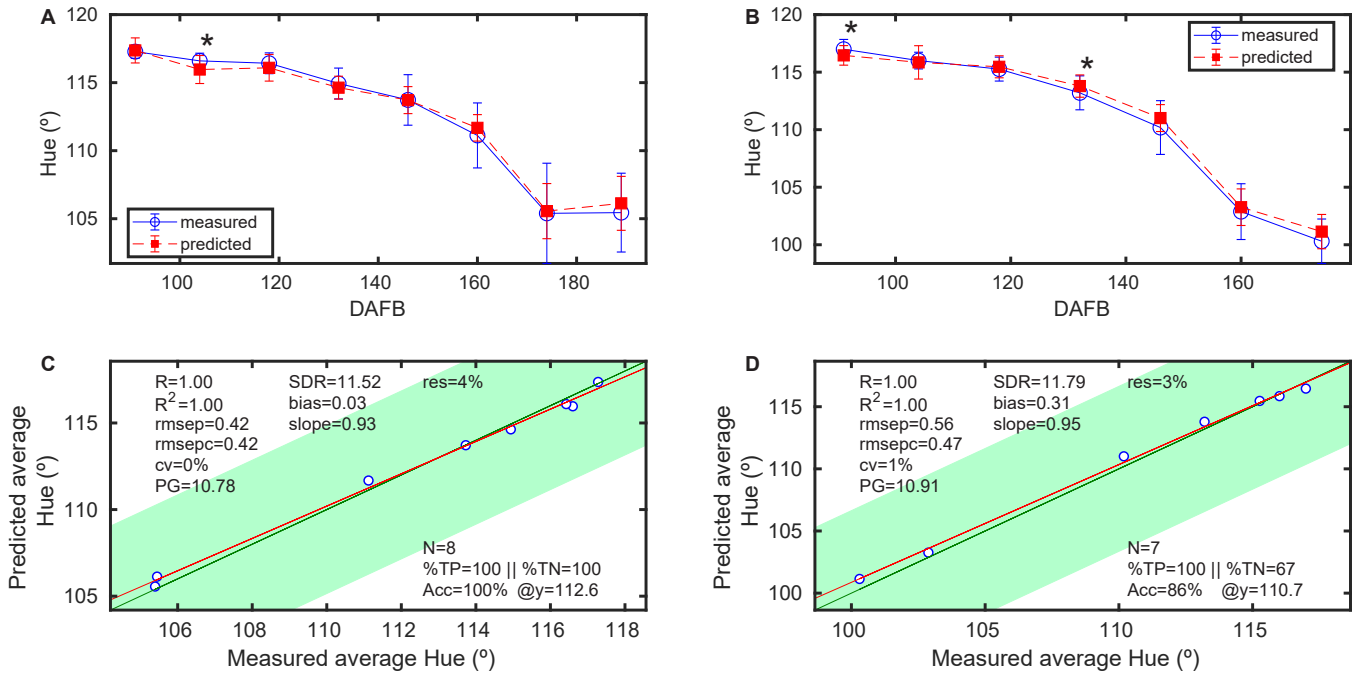

Fig. 5. A: Average measured (open squares / solid line) and predicted (closed squares / dashed line) Hue values for each date in orchard 1 (DAFB = Days After Bloom). Each point represents the mean of the values in each day and the error bars represent their standard deviation. Statistically different means ($p < 0.05$) are signaled with an asterisk. B: same as A, for orchard 2. C: plot of average measured vs. average predicted Hue values and associated prediction statistics for orchard 1. D: same as C, for orchard 2.

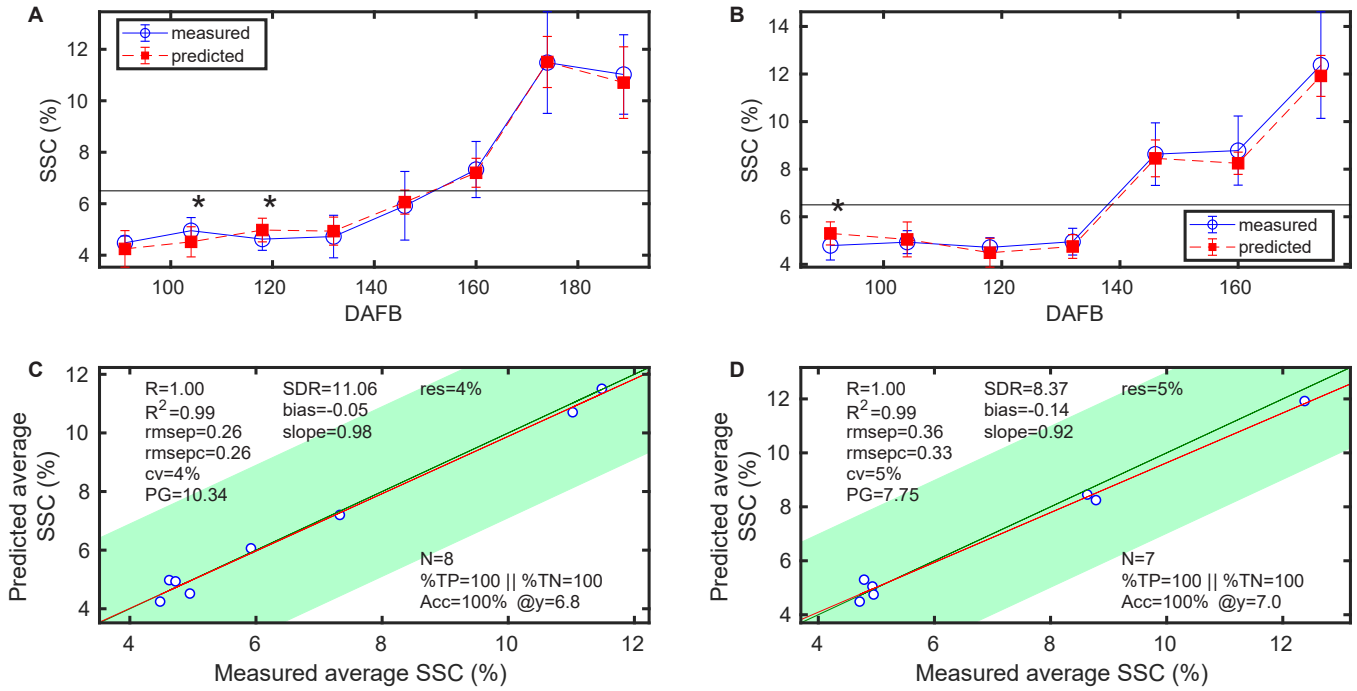

Fig. 6. A: Average measured (open squares / solid line) and predicted (closed squares / dashed line) SSC values for each date in orchard 1 (DAFB = Days After Bloom). Each point represents the mean of the values in each day and the error bars represent their standard deviation. Statistically different means ($p < 0.05$) are signaled with an asterisk. The horizontal line is placed at the minimum mandatory SSC for harvest. B: same as A, for orchard 2. C: plot of average measured vs. average predicted SSC values and associated prediction statistics for orchard 1. D: same as C, for orchard 2.

chlorophyll band, since the current models seem to rely on indirect correlations with it. Another issue of concern is the possibility of having significant bias in the predictions of one year from a model developed in another year, with obvious impact on average predictions.

The final and main conclusion of this work is that there is a very good prospect for the utilization of average predictions for follow-up of ripening in the management of 'Jintao' kiwifruit orchards. Further work is under way to confirm this perspective.

CRediT authorship contribution statement

Andreia M. Afonso: Investigation, Data curation, Formal analysis, Methodology. **M. Dulce Antunes**: Conceptualization, Methodology, Supervision. **Sandra P. Cruz:** Software, Formal analysis. **Ana M. Cavaco**: Conceptualization, Methodology, Writing – review & editing. **Rui Guerra:** Conceptualization, Formal analysis, Data curation, Resources, Software, Visualization, Funding acquisition, Supervision, Roles/ Writing – original draft, Writing – review & editing.

Acknowledgments

The authors acknowledge Frutas Douro ao Minho (Guimarães, Portugal) for providing the access to the orchards followed in this study and FCT - Fundação para a Ciência e a Tecnologia, Portugal, for funding Andreia M. Afonso through a PhD scholarship (SFRH/BD/131462/2017) and for supporting CEOT through the contracts UIDB/00631/2020 CEOT BASE and UIDP/00631/2020 CEOT PROGRAMÁTICO. Part of the work was also supported by the projects NIBAP(ALG-01-0247-FEDER-037303) and OtiCalFrut (ALG-01-0247-FEDER-033652).

Declaration of Competing Interest

The authors declare that they have no known competing financial interests or personal relationships that could have appeared to influence the work reported in this paper.

Appendix A. Supporting information

Supplementary data associated with this article can be found in the online version at doi:10.1016/j.postharvbio.2022.111895.

References

Andersson, M., 2009. A comparison of nine PLS1 algorithms. J. Chemom. 23, 518–529. https://doi.org/10.1002/cem.2736.

Arazuri, S., Jarén, C., Arana, J., 2005. Selection of the temperature in the sugar content determination of kiwi fruit. Int. J. Infrared Millim. Waves 26, 607–616. https://doi.org/10.1007/s10762-005-4076-8.

Barnes, R., Dhanoa, M.S., Lister, S.J., 1989. Standard normal variate transformation and de-trending of near-infrared diffuse reflectance spectra. Appl. Spectrosc. 43, 772–777. https://doi.org/10.1366/0003702894202201.

Beever, D., Hopkirk, G., Warrington, I., Weston, G., 1990. Fruit Development And Fruit Physiology. 'Kiwifruit: Science and Management. Ray Richards, Auckland, pp. 97–126.

Benelli, A., Cevoli, C., Fabbri, A., Ragni, L., 2021. Ripeness evaluation of kiwifruit by hyperspectral imaging. Biosyst. Eng. https://doi.org/10.1016/j.biosystemseng.2021.08.009.

Berardinelli, A., Benelli, A., Tartagni, M., Ragni, L., 2019. Kiwifruit flesh firmness determination by a NIR sensitive device and image multivariate data analyses. Sens. Actuators A: Phys. 296, 265–271. https://doi.org/10.1016/j.sna.2019.07.027.

Blanke, M.M., 2013. Non-invasive assessment of firmness and NIR sugar (TSS) measurement in apple, pear and kiwi fruit. Erwerbs-Obstbau 55, 19–24. https://doi.org/10.1007/s10341-013-0181-3.

Cavaco, A.M., Cruz, S.P., Antunes, M.D., Guerra, R., Pires, R., Afonso, A.M., Brázio, A., Silva, L., Lucas, M.R., Daniel, M., et al., 2021. Spatiotemporal modelling of the quality and ripening of two cultivars of "Algarve Citrus" orchards at different edaphoclimatic conditions. Postharvest Biol. Technol. 172, 111386 https://doi.org/10.1016/j.postharvbio.2020.111386.

Cavaco, A.M., Pires, R., Antunes, M.D., Panagopoulos, T., Brázio, A., Afonso, A.M., Silva, L., Lucas, M.R., Cadeiras, B., Cruz, S.P., et al., 2018. Validation of short wave near infrared calibration models for the quality and ripening of "Newhall" orange on tree across years and orchards. Postharvest Biol. Technol. 141, 86–97. https://doi.org/10.1016/j.postharvbio.2018.03.013.

Cen, H., Lu, R., Mendoza, F., Beaudry, R.M., 2013. Relationship of the optical absorption and scattering properties with mechanical and structural properties of apple tissue. Postharvest Biol. Technol. 85, 30–38. https://doi.org/10.1016/j.postharvbio.2013.04.014.

Chen, X., Han, W., 2012. Spectroscopic determination of soluble solids content of Qinmei kiwifruit using partial least squares. Afr. J. Biotechnol. 11, 2528–2536. https://doi.org/10.5897/AJB11.3177.

Cheng, N.Y., Chen, C.C., Liang, B.J., Tseng, S.H., 2019. Nondestructive evaluation of apple fruit quality by frequency-domain diffuse reflectance spectroscopy: variations in apple skin and flesh. Appl. Sci. 9, 2355. https://doi.org/10.3390/app9112355.

Ciccoritti, R., Paliotta, M., Amoriello, T., Carbone, K., 2019. FT-NIR spectroscopy and multivariate classification strategies for the postharvest quality of green-fleshed kiwifruit varieties. Sci. Hortic. 257, 108622 https://doi.org/10.1016/j.scienta.2019.108622.

Clark, C., McGlone, V., De Silva, H., Manning, M., Burdon, J., Mowat, A., 2004. Prediction of storage disorders of kiwifruit (Actinidia chinensis) based on visible-NIR spectral characteristics at harvest. Postharvest Biol. Technol. 32, 147–158. https://doi.org/10.1016/j.postharvbio.2003.11.004.

Costa, G., Bonora, E., Fiori, G., Noferini, M., 2010. Innovative non-destructive device for fruit quality assessment, in: VII international symposium on kiwifruit. Acta Hortic. 913, 575–581. https://doi.org/10.17660/ActaHortic.2011.913.78.

Cruz, S., Guerra, R., Brazio, A., Cavaco, A.M., Antunes, D., Passos, D., 2021. Nondestructive simultaneous prediction of internal browning disorder and quality attributes in 'Rocha'pear (Pyrus communis L.) using VIS-NIR spectroscopy. Postharvest Biol. Technol. 179, 111562 https://doi.org/10.1016/j.postharvbio.2021.111562.

Farrés, M., Platikanov, S., Tsakovski, S., Tauler, R., 2015. Comparison of the variable importance in projection (vip) and of the selectivity ratio (sr) methods for variable selection and interpretation. J. Chemom. 29, 528–536. https://doi.org/10.1002/cem.2736.

Fazayeli, A., Kamgar, S., Nassiri, S.M., Fazayeli, H., De la Guardia, M., 2019. Dielectric spectroscopy as a potential technique for prediction of kiwifruit quality indices during storage. Inf. Process. Agric. 6, 479–486. https://doi.org/10.1016/j.inpa.2019.02.002.

Filzmoser, P., Liebmann, B., Varmuza, K., 2009. Repeated double cross validation. J. Chemom.: J. Chemom. Soc. 23, 160–171. https://doi.org/10.1002/cem.1225.

Fu, X., Ying, Y., Lu, H., Xu, H., Yu, H., 2007. FT-NIR diffuse reflectance spectroscopy for kiwifruit firmness detection. Sens. Instrum. Food Qual. Saf. 1, 29–35. https://doi.org/10.1007/s11694-007-9004-2.

Guo, W., Li, W., Yang, B., Zhu, Z., Liu, D., Zhu, X., 2019. A novel noninvasive and cost-effective handheld detector on soluble solids content of fruits. J. Food Eng. 257, 1–9. https://doi.org/10.1016/j.jfoodeng.2019.03.022.

Guo, W., Zhao, F., Dong, J., 2016. Nondestructive measurement of soluble solids content of kiwifruits using near-infrared hyperspectral imaging. Food Anal. Methods 9, 38–47. https://doi.org/10.1007/s12161-015-0165-z.

Javadi, S., Nasiri, S.M., 2017. Application of acoustic method for estimation of kiwifruit firmness during storage. Iran. J. Food Sci. Technol. 13, 143–150.

Kim, J., Park, Y., Shin, M., Muneer, S., Lerud, R., Michelson, C., Kang, D.I., Min, J., Kumarihami, H.C., 2018. Application of NIR-Spectroscopy to predict the harvesting maturity, fruit ripening and storage ability of Ca-chitosan treated baby kiwifruit. J. Stored Prod. Postharvest Res. 9, 44–53. https://doi.org/10.5897/JSPPR2018.0257.

Lee, J.S., Kim, S.C., Seong, K.C., Kim, C.H., Um, Y.C., Lee, S.K., 2012. Quality prediction of kiwifruit based on near infrared spectroscopy. Hortic. Sci. Technol. 30, 709–717. https://doi.org/10.7235/hort.2012.12139.

Lee, S., Sarkar, S., Park, Y., Yang, J., Kweon, G., 2019. Feasibility study for an optical sensing system for hardy kiwi (Actinidia arguta) sugar content estimation. J. Agric. Life Sci. 53, 147–157. https://doi.org/10.14397/jals.2019.53.3.147.

Li, M., Han, D., Liu, W., 2019. Non-destructive measurement of soluble solids content of three melon cultivars using portable visible/near infrared spectroscopy. Biosyst. Eng. 188, 31–39. https://doi.org/10.1016/j.biosystemseng.2019.10.003.

Li, M., Pullanagari, R.R., Pranamornkith, T., Yule, I.J., East, A.R., 2017. Quantitative prediction of post storage 'Hayward' kiwifruit attributes using at harvest Vis-NIR spectroscopy. J. Food Eng. 202, 46–55. https://doi.org/10.1016/j.jfoodeng.2017.01.002.

Li, M., Qian, Z., Shi, B., Medlicott, J., East, A., 2018. Evaluating the performance of a consumer scale SCiOTM molecular sensor to predict quality of horticultural products. Postharvest Biol. Technol. 145, 183–192. https://doi.org/10.1016/j.postharvbio.2018.07.009.

Liu, D., Guo, W., Li, Q., Xie, D., 2019. Relationship of the bulk optical properties in 950–1650 nm wavelength range with internal quality and microstructure of kiwifruit during maturation. Biosyst. Eng. 184, 45–54. https://doi.org/10.1016/j.biosystemseng.2019.05.005.

Malegori, C., Marques, E.J.N., de Freitas, S.T., Pimentel, M.F., Pasquini, C., Casiraghi, E., 2017. Comparing the analytical performances of Micro-NIR and FT-NIR spectrometers in the evaluation of acerola fruit quality, using PLS and SVM regression algorithms. Talanta 165, 112–116. https://doi.org/10.1016/j.talanta.2016.12.035.

McGlone, V.A., Clark, C.J., Jordan, R.B., 2007. Comparing density and VNIR methods for predicting quality parameters of yellow-fleshed kiwifruit (Actinidia chinensis). Postharvest Biol. Technol. 46, 1–9. https://doi.org/10.1016/j.postharvbio.2007.04.003.

McGlone, V.A., Jordan, R.B., 2000. Kiwifruit and apricot firmness measurement by the non-contact laser air-puff method. Postharvest Biol. Technol. 19, 47–54. https://doi.org/10.1016/S0925-5214(00)00068-5.

McGlone, V.A., Jordan, R.B., Seelye, R., Martinsen, P.J., 2002. Comparing density and NIR methods for measurement of Kiwifruit dry matter and soluble solids content. Postharvest Biol. Technol. 26, 191–198. https://doi.org/10.1016/S0925-5214(02)00014-5.

McGlone, V.A., Kawano, S., 1998. Firmness, dry-matter and soluble-solids assessment of postharvest kiwifruit by NIR spectroscopy. Postharvest Biol. Technol. 13, 131–141. https://doi.org/10.1016/S0925-5214(98)00007-6.

McGuire, R.G., 1992. Reporting of objective color measurements. HortScience 27, 1254–1255. https://doi.org/10.21273/HORTSCI.27.12.1254.

Mishra, P., Rutledge, D.N., Roger, J.M., Wali, K., Khan, H.A., 2021. Chemometric pre-processing can negatively affect the performance of near-infrared spectroscopy models for fruit quality prediction. Talanta 229, 122303. https://doi.org/10.1016/j.talanta.2021.122303.

Moghimi, A., Aghkhani, M.H., Sazgarnia, A., Sarmad, M., 2010. Vis/NIR spectroscopy and chemometrics for the prediction of soluble solids content and acidity (pH) of kiwifruit. Biosyst. Eng. 106, 295–302. https://doi.org/10.1016/j.biosystemseng.2010.04.002.

Musacchi, S., Serra, S., 2018. Apple fruit quality: Overview on pre-harvest factors. Sci. Hortic. 234, 409–430. https://doi.org/10.1016/j.scienta.2017.12.057.

Nicolaï, B.M., Beullens, K., Bobelyn, E., Peirs, A., Saeys, W., Theron, K.I., Lammertyn, J., 2007. Nondestructive measurement of fruit and vegetable quality by means of NIR spectroscopy: a review. Postharvest Biol. Technol. 46, 99–118. https://doi.org/10.1016/j.postharvbio.2007.06.024.

Nie, S., AlRiza, D.F., Ogawa, Y., Suzuki, T., Kuramoto, M., Miyata, N., Kondo, N., 2020. Potential of a double lighting imaging system for characterization of 'hayward' kiwifruit harvest indices. Postharvest Biol. Technol. 162, 111113 https://doi.org/10.1016/j.postharvbio.2019.111113.

Oja, H., 2010. Multivariate Nonparametric Methods with R: an Approach Based on Spatial Signs and Ranks. Springer Science & Business Media. https://doi.org/10.1007/978-1-4419-0468-3.

Pourkhak, B., Mireei, S.A., Sadeghi, M., Hemmat, A., 2017. Multi-sensor data fusion in the nondestructive measurement of kiwifruit texture. Measurement 101, 157–165. https://doi.org/10.1016/j.measurement.2017.01.024.

Qin, J., Lu, R., 2008. Measurement of the optical properties of fruits and vegetables using spatially resolved hyperspectral diffuse reflectance imaging technique. Postharvest Biol. Technol. 49, 355–365. https://doi.org/10.1016/j.postharvbio.2008.03.010.

Ragni, L., Berardinelli, A., Guarnieri, A., 2010. Impact device for measuring the flesh firmness of kiwifruits. J. Food Eng. 96, 591–597. https://doi.org/10.1016/j.jfoodeng.2009.09.006.

Ragni, L., Cevoli, C., Berardinelli, A., Silaghi, F.A., 2012. Non-destructive internal quality assessment of "Hayward" kiwifruit by waveguide spectroscopy. J. Food Eng. 109, 32–37. https://doi.org/10.1016/j.jfoodeng.2011.10.002.

Rocchi, L., Vidoni, S., Ceccarelli, A., Fiori, G., Costa, G., 2016. Use of the DAindex TM for monitoring fruit ripening evolution in A. chinensis to precisely assess harvesting time "in planta". J. Berry Res. 6, 373–379. https://doi.org/10.3233/JBR-160116.

Sarkar, S., Basak, J.K., Moon, B.E., Kim, H.T., 2020. A comparative study of PLSR and SVM-R with various preprocessing techniques for the quantitative determination of soluble solids content of hardy kiwi fruit by a portable Vis/NIR spectrometer. Foods 9, 1078. https://doi.org/10.3390/foods9081078.

Savitzky, A., Golay, M.J.E., 1964. Smoothing and differentiation of data by simplified least squares procedures. Anal. Chem. 36, 1627–1639. https://doi.org/10.1021/ac60214a047.

Schaare, P., Fraser, D., 2000. Comparison of reflectance, interactance and transmission modes of visible-near infrared spectroscopy for measuring internal properties of kiwifruit (it Actinidia chinensis). Postharvest Biol. Technol. 20, 175–184. https://doi.org/10.1016/S0925-5214(00)00130-7.

Schröder, R., Atkinson, R.G., 2006. Kiwifruit cell walls: towards an understanding of softening? N. Z. J. For. Sci. 36, 112.

Shibang, M., 2021. Nondestructive determination of kiwifruit SSC using visible/near-infrared spectroscopy with genetic algorithm. J. Eng. Sci. Technol. Rev. 14. https://doi.org/10.25103/jestr.141.11.

Tang, M., Cai, J., Lu, H., Chaitep, S., et al., 2010a. Selection of efficient wavelengths in NIR spectrum for determination of dry matter in kiwi fruit. Maejo Int. J. Sci. Technol. 4, 113–124.

Tang, M., Cai, J., Lu, H., et al., 2010b. Long-term prediction of zhonghua kiwifruit dry matter by near infrared spectroscopy. Scienceasia 36, 210–215. https://doi.org/10.2306/scienceasia1513-1874.2010.36.210.

Testolin, R., Ferguson, A., 2009. Kiwifruit (Actinidia spp.) production and marketing in Italy. N. Z. J. Crop Hortic. Sci. 37, 1–32. https://doi.org/10.1080/01140670909510246.

Vieira, A., Guerreiro, A., Gago, C., Brázio, A., Guerra, R., Cavaco, A., Panagopoulos, T., Veloso, F., Antunes, M., 2017. An attempt to find a non-destructive method to determine ripeness of kiwifruit (Actinidia chinensis Planch. "Jintao'), in: IX international symposium on kiwifruit. Acta Hortic. 1218, 489–496. https://doi.org/10.17660/ActaHortic.2018.1218.67.

Walsh, K., McGlone, V., Han, D., 2020a. The uses of near infra-red spectroscopy in postharvest decision support: a review. Postharvest Biol. Technol. 163, 111139 https://doi.org/10.1016/j.postharvbio.2020.111139.

Walsh, K.B., Blasco, J., Zude-Sasse, M., Sun, X., 2020b. Visible-NIR "point' spectroscopy in postharvest fruit and vegetable assessment: the science behind three decades of commercial use. Postharvest Biol. Technol. 168, 111246 https://doi.org/10.1016/j.postharvbio.2020.111246.

Zhu, H., Chu, B., Fan, Y., Tao, X., Yin, W., He, Y., 2017. Hyperspectral imaging for predicting the internal quality of kiwifruits based on variable selection algorithms and chemometric models. Sci. Rep. 7, 1–13. https://doi.org/10.1038/s41598-017-08509-6.